Microstructure, optical, and electrical properties of *p*-type SnO thin films

W. Guo,[1] L. Fu,[1,a)] Y. Zhang,[1] K. Zhang,[1] L. Y. Liang,[2] Z. M. Liu,[2] H. T. Cao,[2] and X. Q. Pan[1,b)]
[1]*Department of Materials Science and Engineering, University of Michigan, Ann Arbor, Michigan 48109-2136, USA*
[2]*Division of Functional Materials and Nano Devices, Ningbo Institute of Materials Technology and Engineering, Chinese Academy of Sciences, Ningbo 315201, People's Republic of China*

(Received 27 July 2009; accepted 12 October 2009; published online 29 January 2010)

SnO thin films were fabricated by electron beam evaporation on (100) Si and *c*- and *r*-plane Al_2O_3 substrates. The films grown at 25 °C are nanocrystalline, while the films grown at 600 °C are epitaxial on *r*-plane Al_2O_3 and (001) textured on Si and *c*-plane Al_2O_3. The SnO films have an optical band gap of 2.82–2.97 eV and *p*-type conductivity, according to Hall measurements, with resistivities of 0.5–110 Ω cm, hole concentrations of 10^{17}–10^{19} cm^{-3}, and Hall mobilities of 0.1–2.6 cm^2/Vs. The *p*-type conductivity, which appears to correlate with V_{Sn}, can be enhanced via Y- and Sb-doping. Defect complexes of $Sb_{Sn}-2V_{Sn}$ are suggested to be the acceptors in Sb-(or Y-) doped SnO films. © *2010 American Institute of Physics*. [doi:10.1063/1.3277153]

Research on tin oxides has long been focused on tin dioxide (SnO_2), a stable wide band-gap semiconductor with the rutile structure, widely used in applications such as gas sensors, transparent electrodes, and solar cells.[1,2] By contrast, there are fewer experimental reports on tin monoxide (SnO), due to its metastability with respect to transformation into SnO_2 at high oxygen pressure.[3,4] In recent years, however, SnO has received greater attention because it, too, has a wide optical band gap of 2.7–3.4 eV,[5] but in contrast to the *n*-type behavior of SnO_2, SnO exhibits *p*-type conductivity.[6,7] Since the only reported *p*-type wide band-gap semiconducting oxides are either copper oxide compounds[8,9] or ZnO with *p*-type doping,[10] this property of SnO makes it an interesting candidate for optoelectronic applications. Recently, Ogo *et al.*[6] reported *p*-channel TFTs based on epitaxial SnO films grown on yttria-stabilized zirconia substrates, promising for organic light emitting devices.

Although SnO has received more attention recently, the physical properties of SnO have not been investigated in detail. There are only a few reports focused on its *p*-type conductivity,[6,7] and no studies of the effects of doping on its electrical transport properties have been reported. In this work, we studied the microstructure and properties of both undoped and doped SnO thin films grown on Si and Al_2O_3 substrates by electron beam evaporation. We found that the SnO films are stable, maintaining both structure and *p*-type conductivity over a period of six years. The effects of doping with yttrium and antimony on the electrical transport properties were also investigated.

SnO thin films were deposited from a high purity SnO_2 ceramic source by electron beam evaporation onto (100) Si and both (0001) and ($\bar{1}012$) Al_2O_3 (*c*-plane and *r*-plane Al_2O_3, respectively) substrates. The (100) Si substrates have a SiO_2 cap layer 300 nm thick. We also deposited doped SnO thin films with nominal 1–5 at. % Y- or Sb-doping by mixing the SnO_2 source with Y_2O_3 or Sb_2O_3, respectively. The films were deposited at room temperature (~25 °C), 350, and 600 °C, with nominal thicknesses of around 100 nm. Details of the deposition procedures and source material preparation have been reported previously.[7] We would like to emphasize that all data presented in this paper were obtained over the past 12 months, approximately six years after the films were fabricated. During this six-year period, all films were stored in vacuum desiccators.

Figure 1 shows typical x-ray diffraction (XRD) patterns in θ-2θ scans of the SnO films grown at 600 and 25 °C on all three substrates. The doped SnO films show similar patterns. In each pattern, in addition to the strong substrate peaks, there are three sharp peaks, located at 18.3°, 37.2°, and 79.2°, corresponding to the 001, 002, and 004 reflections of the tetragonal α-SnO phase (space group $P4/nmm$). Small peaks corresponding to the 101 (29.9°), 110 (33.2°), and 211 (57.3°) reflections of SnO are also seen on the log scale for the films grown on (100) Si and *c*-plane Al_2O_3 but they are barely distinguishable for the films grown at 600 °C on *r*-plane Al_2O_3 [Fig. 1(c)]. Figures 1(a)–1(c) imply that the SnO films grown at 600 °C on (100) Si and *c*-plane Al_2O_3

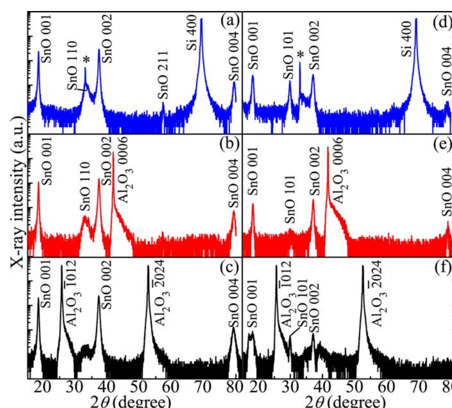

FIG. 1. (Color online) XRD θ-2θ scans (on a log scale) of the SnO films grown on (100) Si, (0001) Al_2O_3, and ($\bar{1}012$) Al_2O_3 substrates at 600 °C [(a)–(c)] and 25 °C [(d)–(f)], respectively. The "*" signs in (a) and (d) denote a residual peak (33°) induced from the Si substrates.

a)Present Address: Advanced Micro-Fabrication Equipment, Inc., CA.
b)Author to whom correspondence should be addressed. Electronic mail: panx@umich.edu.

 © 2010 American Institute of Physics

Downloaded 31 Jan 2010 to 130.237.29.138. Redistribution subject to AIP license or copyright; see http://apl.aip.org/apl/copyright.jsp

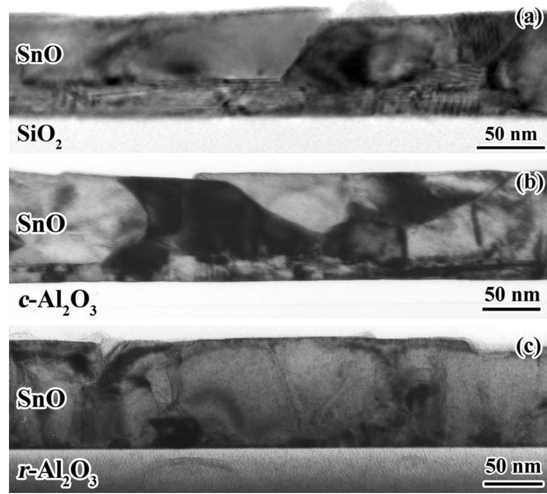

FIG. 2. Cross-sectional TEM images of the SnO films grown at 600 °C on (a) (100) Si, (b) (0001) Al_2O_3, and (c) $(\bar{1}012)$ Al_2O_3 substrates.

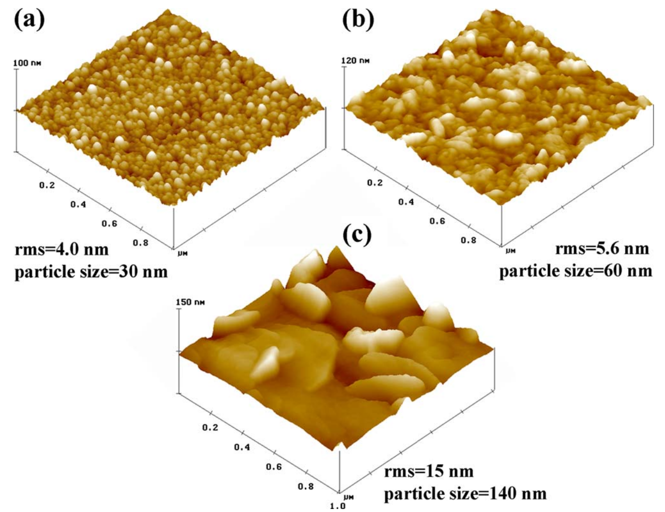

FIG. 3. (Color online) AFM images of SnO films grown on (100) Si substrates at (a) 25 °C, (b) 350 °C, and (c) 600 °C.

are polycrystalline, but strongly 001 textured, whereas the films grown on *r*-plane Al_2O_3 are epitaxial with an orientation relationship of $(001)[100]_{SnO} \| (\bar{1}012)[2\bar{2}01]_{Al_2O_3}$ as originally found in previous transmission electron microscopy (TEM) studies.[7] The measured full-width-at-half-maximum value of the 001 SnO ω-rocking curve was 2.9° for the films grown on *r*-plane Al_2O_3 at 600 °C. In the XRD patterns of the films grown at 25 °C [Figs. 1(d)–1(f)], the SnO peaks have lower intensities, but no peaks from SnO_2 or other impurity phase were observed within the instrumental detection limit. These results agree with the previous XRD data measured from fresh films,[7] suggesting that the SnO thin films studied in this work have high structural stability, allowing them to remain unchanged under storage for a period of at least six years.

The cross-sectional TEM images of the 600 °C grown SnO films shown in Fig. 2 corroborate the microstructure deduced from the XRD results. The films grown on (100) Si and *c*-plane Al_2O_3 [Figs. 2(a) and 2(b), respectively] show various grain sizes between 100 and 150 nm. These films are polycrystalline because there is no epitaxial relationship between the films and the substrates. The SnO films grown on *r*-plane Al_2O_3 are epitaxial, however, because the *r*-plane of Al_2O_3 has a pseudocubic symmetry and a small lattice mismatch of 7.6% with SnO.[7] Figure 2(c) shows that there are many threading dislocations in the SnO films grown on *r*-plane Al_2O_3, propagating from the interface into the film, ending at surface pits. According to TEM results (not shown), the films grown at 350 and 25 °C are polycrystalline and nanocrystalline, respectively, with no preferred out-of-plane orientation on any of the three substrates.

The surface morphologies of the SnO films were investigated by atomic force microscopy (AFM). Figure 3 shows the AFM images of the films grown on (100) Si at 25, 350, and 600 °C. (The films grown on *c*-plane and *r*-plane Al_2O_3 have similar surface morphologies.) The films grown at 25 °C have smooth surfaces, comprising small nanocrystals, while the films grown at 600 °C have rough surfaces, comprising large randomly faceted grains. The root mean square (RMS) surface roughness ranges from 4.0 nm (25 °C) to 15 nm (600 °C), while the average grain size ranges from 30 to 140 nm accordingly. The transition of the surface morphology can be explained by enhanced atom diffusion on the surface with increasing temperature, which enables more effective long-range crystal ordering. The crystal grains grow along low stress directions, resulting in faceted surface shapes and larger RMS roughness for the films grown at higher temperature.

All SnO films have a light yellowish color with an average optical transparency of 70%–85% as shown in the optical transmittance spectrum in Fig. 4. No noticeable color change of the films has been observed while under storage. Photoluminescence (PL) spectra, measured using a He-Cd laser ($\lambda = 325$ nm), are also shown in Fig. 4. A representative room temperature PL spectrum of 600 °C grown films peaks at 440 nm, which is in accordance with the absorption edge of the transmittance spectrum. The direct optical band gap of SnO obtained from the PL spectrum is 2.82 eV (440 nm), closely matching the value determined from the Tauc plot of $(\alpha h\nu)^2$ versus $h\nu$ (inset of Fig. 4). The optical band gap slightly blueshifts in temperature-dependent PL measurements to 2.85 eV (435 nm) at 10 K. (Interference fringes in the PL spectrum were introduced by a long wave edge pass filter in the PL set up.) Figure 4 also includes a typical room temperature PL spectrum of 25 °C grown films. Because of the nanocrystallinity of these films, the spectrum intensity is much lower than that of the 600 °C grown films. The optical band gap blueshifts to 2.97 eV (418 nm), indicating a de-

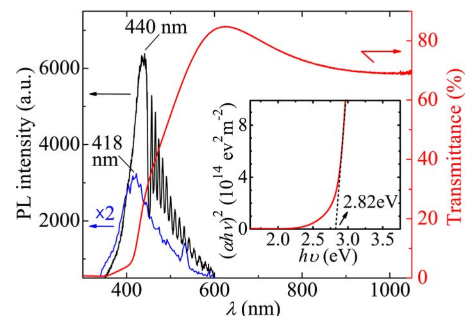

FIG. 4. (Color online) Representative PL and optical transmittance spectra measured at room temperature. The transmittance and high intensity PL spectra are from a 600 °C grown SnO film. The low intensity (×2) PL spectrum is from a 25 °C grown film. The inset is a Tauc plot of $(\alpha h\nu)^2$ vs $h\nu$ obtained from the transmittance spectrum.

Downloaded 31 Jan 2010 to 130.237.29.138. Redistribution subject to AIP license or copyright; see http://apl.aip.org/apl/copyright.jsp

TABLE I. Comparison of room temperature electrical properties of SnO films grown on different substrates at 25 and 600 °C.

Films on	T_G (°C)	[Sn]/[O] (±0.02)	Type	ρ (Ω cm)	n_{holes} (cm^{-3})	μ ($cm^2/V s$)
SiO_2/(100) Si	25	0.38/0.62	*p*	0.5	5.0×10^{18}	2.6
	600	0.43/0.57	*p*	35	7.3×10^{17}	0.3
(0001) Al_2O_3	25	0.43/0.57	*p*	4.8	1.4×10^{18}	1.0
	600	0.48/0.52	*p*	53	5.7×10^{16}	2.1
($\bar{1}$012) Al_2O_3	25	0.40/0.60	*p*	0.6	8.6×10^{19}	0.1
	600	0.48/0.52	*p*	110	5.6×10^{17}	0.1

TABLE II. Comparison of room temperature electrical properties of the undoped, Y-, and Sb-doped SnO films grown at 350 °C.

Substrate	Doping	Type	ρ (Ω cm)	n_{holes} (cm^{-3})	μ ($cm^2/V s$)
SiO_2/(100) Si	undoped	*p*	43	8.0×10^{17}	0.2
	1 at. % Y	*p*	12	3.1×10^{17}	1.7
	5 at. % Y	*p*	2.4	1.1×10^{18}	3.6
($\bar{1}$012) Al_2O_3	undoped	*p*	7.1	1.1×10^{18}	0.8
	5 at. % Y	*p*	3.8	2.7×10^{18}	0.6
	5 at. % Sb	*p*	5.5	1.3×10^{18}	0.9

crease in the density of color center defects such as oxygen vacancies. Note that the optical band gap is much smaller than that of SnO_2 (~3.6 eV), consistent with XRD results indicating that no significant amount of SnO_2 exists in the films.

Electrical properties of the SnO films were obtained by four-point Hall measurements made at room temperature using the van der Pauw configuration. Table I compares the electrical properties of the 25 and 600 °C grown films on all three substrates. (We also include the atomic concentration ratio of tin to oxygen ([Sn]/[O]) obtained by RBS measurements and simulations using SIMNRA[11] software.) Regardless of the substrate, growth temperature, or microstructure, all films exhibit *p*-type conductivity. The highest mobility value measured was 2.6 $cm^2/V s$ for the nanocrystalline films grown on Si substrates, comparable to the value (2.4 $cm^2/V s$) reported for the SnO-channel TFT device.[6] Comparing the films grown on the same substrate at 600 °C to those grown at 25 °C, the resistivities increase and hole concentrations decrease by one to two orders of magnitude.

Many factors, such as microstructure and strain, can affect carrier transport in thin films. In this letter, the effect of stoichiometry (i.e., [Sn]/[O] ratio) is considered. The RBS results in Table I show that all films grown at 25 °C contain less tin (relative to oxygen) than those grown at 600 °C on a given substrate. Togo *et al.*[12] suggested that tin vacancies (V_{Sn}) are the dominant shallow acceptors. We expect that increasing oxygen concentration in the films drive down the formation energy of V_{Sn} and drive them to the grain boundaries, which are of high densities in the 25 °C grown films. Therefore, a SnO film with high [O] favors the formation of V_{Sn} acceptors which thus produces more mobile holes. This conclusion is also in agreement with the fact that on the same substrate, the *p*-type SnO films grown at 25 °C with lower [Sn]/[O] ratios are more conductive than those grown at 600 °C with higher [Sn]/[O] ratios.

The *p*-type conductivity of the SnO films can be further enhanced via doping. Table II compares the electrical properties of undoped, Y-doped, and Sb-doped SnO films grown at 350 °C on (100) Si and *r*-plane Al_2O_3 substrates. On (100) Si, as the concentration of Y-doping increases, the resistivity of the *p*-type SnO film drops more than one order of magnitude from 43 Ω cm (undoped) to 2.4 Ω cm (5 at. % Y-SnO). The hole concentration of the film first drops from 8.0×10^{17} (undoped) to 3.1×10^{17} cm^{-3} (1 at. % Y-SnO), and it then rises to 1.1×10^{18} cm^{-3} (5 at. % Y-SnO). With 5 at. % Y-doping, the mobility value is enhanced to 3.6 $cm^2/V s$. On *r*-plane Al_2O_3, the film conductivity and hole concentration are all improved by 5 at. % Y- or Sb-doping but the mobility remains small (<1.0 $cm^2/V s$).

We suggest a doping mechanism of SnO similar to that proposed by Limpijumnong *et al.*[13] for doping of ZnO. When doped into SnO, large size dopants such as Sb (or Y) easily substitute Sn, and form the defects of Sb_{Sn}^{3+} which act as donors. Then Coulomb binding between Sb_{Sn}^{3+} and the native defects, V_{Sn}^{2-}, results in the formation of charged defect complexes; $Sb_{Sn}^{3+}+V_{Sn}^{2-}+V_{Sn}^{2-}\rightarrow(Sb_{Sn}-2V_{Sn})^-$, and these defect complexes act as acceptors. When 1 at. % Y-doping is incorporated into the SnO film on (100) Si, donors Y_{Sn}^{3+} form first, leading to the initial drop of the hole concentration. When Y-doping is increased to 5 at. %, the hole concentration rises because acceptor complexes gradually form and produce excess mobile holes. The enhancement of Hall mobility upon doping is induced by an increase in grain size probably because the dopants promote the grain growth rate. On *r*-plane Al_2O_3, the small mobility values are too close to the accuracy limit of our Hall measurements to allow any conclusions regarding the doping effects.

This work was supported by the National Science Foundation through grants DMR-0907191 and DMR-0315633 and by the Department of Energy through grant DE-FG02–07ER46416. The authors would like to thank G. W. Graham and M. B. Katz for their critical reading of this paper.

[1] K. Ihokura and J. Watson, *The Stannic Oxide Gas Sensor: Principles and Applications* (CRC, Boca Raton, 1994).
[2] K. Hara, T. Horiguchi, T. Kinoshita, K. Sayama, H. Sugihara, and H. Arakawa, Sol. Energy Mater. Sol. Cells **64**, 115 (2000).
[3] M. R. Soares, P. H. Dionísio, I. J. R. Baumvol, and W. H. Schreiner, Thin Solid Films **214**, 6 (1992).
[4] X. Q. Pan and L. Fu, J. Appl. Phys. **89**, 6048 (2001).
[5] R. Sivaramasubramaniam, M. R. Muhamad, and S. Radhakrishna, Phys. Status Solidi A **136**, 215 (1993).
[6] Y. Ogo, H. Hiramatsu, K. Nomura, H. Yanagi, T. Kamiya, M. Hirano, and H. Hosono, Appl. Phys. Lett. **93**, 032113 (2008).
[7] X. Q. Pan and L. Fu, J. Electroceram. **7**, 35 (2001).
[8] H. Kawazoe, M. Yasukawa, H. Hyodo, M. Kurita, H. Yanagi, and H. Hosono, Nature (London) **389**, 939 (1997).
[9] A. Kudo, H. Yanagi, H. Hosono, and H. Kawazoe, Appl. Phys. Lett. **73**, 220 (1998).
[10] A. Tsukazaki, A. Ohtomo, T. Onuma, M. Ohtani, T. Makino, M. Sumiya, K. Ohtani, S. F. Chichibu, S. Fuke, Y. Segawa, H. Ohno, H. Koinuma, and M. Kawasaki, Nature Mater. **4**, 42 (2005).
[11] M. Mayer, *SIMNRA User's Guide 6.0*. (http://www.rzg.mpg.de/~mam/, Max-Planck-Institut für Plasmaphysik, Garching, Germany, 2008).
[12] A. Togo, F. Oba, I. Tanaka, and K. Tatsumi, Phys. Rev. B **74**, 195128 (2006).
[13] S. Limpijumnong, S. B. Zhang, S.-H. Wei, and C. H. Park, Phys. Rev. Lett. **92**, 155504 (2004).

Downloaded 31 Jan 2010 to 130.237.29.138. Redistribution subject to AIP license or copyright; see http://apl.aip.org/apl/copyright.jsp